RSC Advances

ROYAL SOCIETY OF CHEMISTRY

www.rsc.org/advances

天津大学
Tianjin University

No. 92 weijin Road, Nankai District, Tianjin 300072, PR China

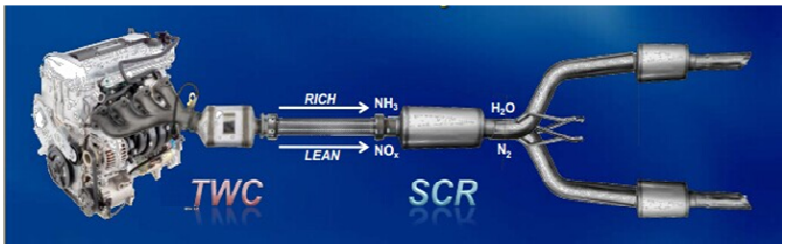

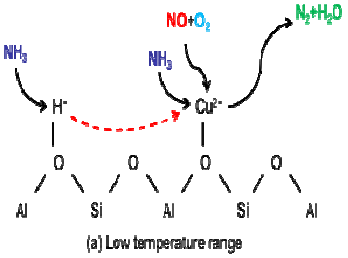

(a) Low temperature range

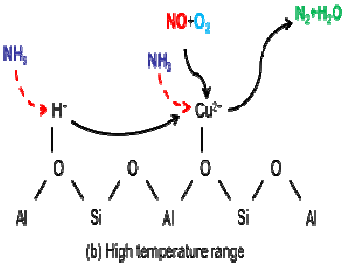

(b) High temperature range

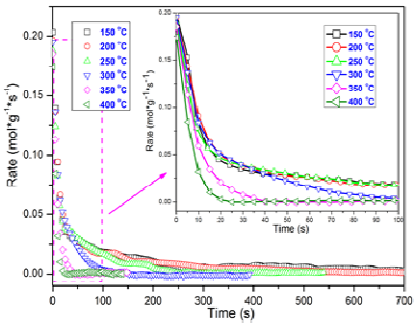

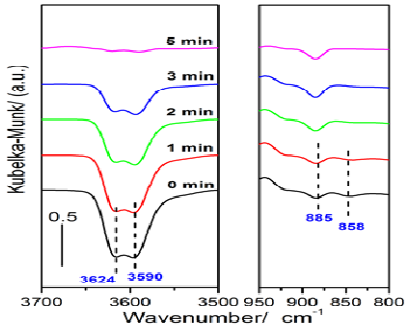

The Role and Activity of Various Adsorbed Ammonia Species on Cu/SAPO-34 Catalyst during Passive-SCR Process

Yingfeng Duan, [a] Jun Wang, [a] Tie Yu, [a] Meiqing Shen, [*a, b, c] and Jianqiang Wang [*a]

[a] Key Laboratory for Green Chemical Technology of State Education Ministry, School of Chemical Engineering & Technology, Tianjin University, Tianjin 300072, PR China

[b] Collaborative Innovation Center of Chemical Science and Engineering (Tianjin), Tianjin 300072, PR China

[c] State Key Laboratory of Engines, Tianjin University, Tianjin 300072, PR China

* Corresponding author: Meiqing Shen, Jianqiang Wang

Postal address:

School of Chemical Engineering and Technology, Tianjin University, 92 Weijin Road, Nankai District, Tianjin 300072, China

Email: jianqiangwang@tju.edu.cn; mqshen@tju.edu.cn

Tel. / Fax. : (+86) 22-27407002

Abstract

In this work, adsorption and reaction performance of various adsorbed ammonia species during passive-SCR process were investigated by temperature-programmed desorption (TPD), temperature-fixed surface reaction (TFSR), *in situ* diffuse reflectance infrared Fourier transform spectroscopy (*in situ* DRIFTS) and kinetic tests. NH_3-TPD and DRIFTS-NH_3 adsorption results showed that the amount of weak and strong acid sites in Cu/SAPO-34 sample increased due to Cu species incorporation, which formed new Lewis acid sites. And decrease of moderate acid sites resulted from replacement of hydroxyls by Cu^{2+}. TFSR results revealed that adsorbed NH_3 species presented different SCR activity, which could be divided into active NH_3 species and inactive NH_3 species. At low temperature range, massive inactive NH_3 preformed lower activity and resulted in a long equilibrium process. However, the performance of inactive NH_3 was distinctly different at high temperature. Furthermore, *in situ* DRIFTS results illustrated the activity difference and migration between the two adsorbed NH_3 species. It was proved that NH_3 migration rate from Brønsted acid sites to Lewis acid sites was slower than SCR rate at low temperature, which might determine SCR reaction rates. While at high temperature, the NH_3 migration rate was faster than SCR rate of active NH_3. In a word, NH_3 migration from Brønsted acid sites to Lewis acid sites may be rate determining step of passive-SCR lean period at low temperature, while NH_3 adsorption possibly was rate determining step of passive-SCR rich period at high temperature. On the basis of above results, present work gives

insight into potential of Cu/SAPO-34 for passive-SCR application in future.

1. Introduction

Lean burn engine exhibits significant potential for improving fuel efficiency, economy savings and reducing greenhouse gas emissions.[1,2] However, with the more and more strict emission regulations, lean period NO_x generation beyond the regulations has restricted its wide applications.[3-5] Existing de-NO_x strategy requires combination of various technologies, such as two of the most promising solutions under oxygen-rich condition: lean NO_x trap (LNT) and ammonia selective catalytic reduction (NH_3-SCR).[1,6] Nevertheless, both technologies suffer considerable drawbacks due to demanding supporting facility and increasing the cost of aftertreatment system.[7,8] Recently, an efficient and less cost lean NO_x aftertreatment technology reported by Li *et al*. was the passive selective catalytic reduction (passive-SCR),[1] which could replace the complex combination form of various catalysts. Passive-SCR system itself contains two catalysts section of TWC catalyst and NH_3-SCR catalyst. During the rich period, NH_3 is produced on the upstream TWC catalyst and stored on the downstream SCR catalyst. Subsequently, the generated NO_x during lean condition could be consumed by adsorbed NH_3 on downstream SCR catalyst.[3] Considering the dual role of SCR catalyst in passive-SCR system, strong NH_3 adsorption and storage capacity is necessary to trap ammonia during the rich operation avoiding NH_3-slip. Sequently, a high SCR activity may ensure NO_x elimination from lean period. On the basis of above two aspects requirement, Cu/SAPO-34 catalyst shows potential advantages,

compared with traditional ZSM-5 and Beta zeolite catalysts, due to its acidity, excellent SCR activity, high N_2 selectivity and hydrothermal stability in passive-SCR system.[9-16]

Brønsted and Lewis acid sites existing in Cu/SAPO-34 catalysts (chabazite structure) are necessary and important for NH_3 adsorption.[17] The Brønsted acid sites were generated by the isomorphous substitution of P by Si in AlPOs, which played an important role in binding and activating NH_3 to react with NO_x.[18] Lewis acid sites were generated by exchanging the hydroxyls (Al-OH-Si) by Cu^{2+}ions in Cu/SAPO-34 sample.[19,20] Previous NH_3-TPD results have been reported to assign the acidity of SAPO-34 and were compared with different silica-alumina zeolites.[20-24] It provides us important information about contribution of different zeolite structure to acid sites and metal ion incorporation effect on acidity. In addition, titration experiments of adsorbed NH_3 were performed to speculate the mechanism of NH_3-SCR reaction and Lewis acid sites were proposed to be SCR reaction active sites.[21] Furthermore, Wang *et al.* found the NH_3 migration issue and conjectured the existing of NH_3 migration phenomenon.[22] Combining the above evolution, they supply us useful information of basic acid sites and their properties. With respect to passive-SCR process, there is no systematical research about NH_3 adsorption behavior on various acid sites and their reaction performance. Whether Cu/SAPO-34 catalyst can be applied and meet the requirement need to be verified. Especially, reaction mechanism and rate-determining step of passive-SCR process have not been proposed up to now. Consequently, it is

worthy to study adsorption and reaction behavior of ammonia species on Cu/SAPO-34 catalyst, and shed light on guideline for passive-SCR research.

In the present research, H/SAPO-34 support and Cu/SAPO-34 sample were synthesized to investigate the reaction performance of NH_3, NO and O_2 on Cu/SAPO-34 catalyst. NH_3-TPD and DRIFTS test were performed to clarify adsorption sites of NH_3 species and the acid sites variation for Cu incorporation. Furthermore, TFSR and *in situ* DRIFTS experiments were applied to probe into the reactivity of active and inactive ammonia species on various adsorption sites. The NH_3 migration between different acid sites was also researched. Finally, kinetic test was employed to explore possible rate determining step of passive-SCR reaction and give an in-depth understanding about future passive-SCR application.

2. Experiments

2.1 Catalyst preparation

H/SAPO-34 was synthesized via hydrothermal method with mole composition of 0.2 morpholine (MA): 0.1 Al_2O_3: 0.1 P_2O_5: 0.06 SiO_2: 6.4 H_2O. The sources of Si, P and Al were silica sol, 85% phosphoric acid and pseudoboehmite, respectively. Firstly, the pseudoboehmite and phosphoric acid were mixed with water. The mixture was fiercely stirred for 1 h. Secondly, the MA and silica sol were mingled well and dropwise added into the former mixture. Thirdly, the blend was sealed in 200 mL Teflon-lined stainless steel pressure vessels and heated in an oven at 200 ˚C under autogenic pressure for 48 h. Finally, the H/SAPO-34 was obtained through centrifugal

105 separation, washed, dried at 100 ˚C overnight and calcined at 650 ˚C in air for 6 h.
106 Cu/SAPO-34 catalyst was prepared by the ion-exchange method over H/SAPO-34
107 molecular sieve as following. Firstly, NH_4/SAPO-34 was obtained by exchanging
108 H/SAPO-34 in ammonium nitrate solution at 80 ˚C for 3 h. Secondly, NH_4/SAPO-34
109 was added into the copper sulfate solution then stirred at 70 ˚C for 4 h. The slurry was
110 filtered, washed and dried at 90~100 ˚C for 16 h. The dried Cu/SAPO-34 was
111 calcined at 500 ˚C for 5 h. And the aged Cu/SAPO-34 was obtained by 750 ˚C, 10%
112 H_2O, 12 h hydrothermal treatment.

113 **2.2 NH_3 adsorption performance and acid sites characterization**

114 NH_3-TPD experiments were performed to evaluate the amount of acid sites under
115 different temperatures. Prior to the following each experiments, the catalysts were
116 pretreated at 500 ˚C for 30 min in 5% O_2/N_2. And then cooled to the test temperatures
117 (80, 150, 200, 250, 300, 350, 400 ˚C) in N_2. At different test temperatures, NH_3 was
118 introduced in 500 ppm NH_3/N_2 until the outlet concentration of NH_3 was stable. The
119 catalysts were purged with N_2 to remove any weakly adsorbed NH_3. Finally, the
120 catalysts were heated from test temperature to 550 ˚C at a ramp rate of 10 ˚C min^{-1}.
121 Diffuse reflectance infrared Fourier transform spectra (DRIFTS) were performed on
122 Nicolet 6700 FTIR equipped with a MCT detector at a resolution of 1 cm^{-1}. Three
123 scans were operated for each spectrum. The total flow rate was 150 mL min^{-1}. Prior to
124 every experiment, the samples were pretreated with 2% O_2 in He at 500 ˚C for 30 min
125 and the background spectra were collected under He at test temperature.

For the NH_3 adsorption experiments, the samples were exposed to 500 ppm NH_3 at 80, 150, 200, 250, 300, 350, 400 ˚C, respectively. For the adsorbed NH_3-SCR experiments, the NH_3 (500 ppm) was firstly introduced into the catalyst until the spectra were stable. Then the catalyst was exposed to (500 ppm) NO and (5%) O_2 until equilibrium attained. These experiments were performed at 150, 200, 250, 300 and 350 ˚C, respectively.

2.3 NO_x removal performance

2.3.1 de-NO_x efficiency

The SCR activity was tested in a quartz reactor (20 mm inner diameter), in which 0.1 g sample (60~80 mesh) mixed with 0.9 g quartz (60~80 mesh) at atmosphere pressure. The sample was sealed in reactor tube with quartz wool. The K type thermocouple was inserted into the center of catalyst to control the temperature. A Fourier Transform Infrared (FTIR) spectrometer (MKS-2030) equipped with 5.11 m gas cell was used to measure the concentration of NO, NO_2, N_2O and NH_3. The flow rates in all experiments were controlled at 500 mL min^{-1}. After pretreated, SCR tests were conducted with feed gas composition of 500 ppm NO, 500 ppm NH_3 and 5% O_2. The test temperature range was from 100 ˚C to 550 ˚C with interval of 50 ˚C. The NO conversion was calculated using the following equation:

$$NO\ conversion[\%] = \frac{NO_{inlet} - NO_{outlet}}{NO_{inlet}} \times 100[\%] \quad (1)$$

2.3.2 Lean NO_x reaction performance with adsorbed ammonia

The sample particles size was 80~100 mesh and volume hourly space velocity was 3

600 000 h^{-1}. The reaction temperatures were 150 ˚C，200 ˚C，250 ˚C，300 ˚C，350 ˚C and 400 ˚C. After sample was pretreated, NH_3 adsorption was performed with 500 ppm NH_3 until its outlet concentration was stable. The catalyst purged with N_2 after saturated by NH_3. Finally, the titration reaction was performed by introducing in 500 ppm NO and 5% O_2.

2.4 Kinetic experiment

2.4.1 Reaction kinetic experiment

The NH_3-SCR kinetics experiments were performed in a quartz reactor, mixing 25 mg catalyst with 125 mg quartz sand. A relatively small particles size (80~100 mesh) and volume hourly space velocity (3, 600, 000 h^{-1}) was used in kinetic tests. The inlet gas consisted of 500 ppm NO, 500 ppm NH_3 and 5% O_2, with N_2 as the balance gas. The kinetics steady-state measurements were obtained in two temperatures range: low temperature (160~205 ˚C) and high temperature (360~390 ˚C). The NH_3-SCR reaction rates can be calculated from the NO_x conversion by following equations:

$$rate\left[mole\ NOx \cdot g_{cata}{}^{-1} \cdot s^{-1}\right] = \frac{X_{NO_x}[\%] \times F_{NO_x}\left[L_{(NO_x)} \cdot \min^{-1}\right]}{m_{cata} \times 60\left[s \cdot \min^{-1}\right] \times 22.4\left[L \cdot mole^{-1}\right]} \times \left[mole\ NO_x \cdot g_{cata}{}^{-1} \cdot s^{-1}\right] \quad (2)$$

$$X_{NOx} = NO_x Conversion, \quad [\%]; \quad (3)$$

$$F_{NOx} = NO_x flow\ rate, \left[L(NO_x)\ min^{-1}\right] \quad (4)$$

2.4.2 NH_3 adsorption kinetics experiment

The sample particles size and space velocity were the same with the NH_3-SCR kinetics experiments. At each test temperature, 500 ppm NH_3 was introduced into the

167 reactor until the outlet concentration was steady then purged with N_2. At last, sample

168 was heated from test temperature to 550 ˚C at a ramp rate of 10 ˚C min^{-1}.

169 **3. Results**

170 **3.1 NH_3 adsorption performance and adsorption sites over Cu/SAPO-34 catalyst**

171 3.1.1 NH_3-TPD

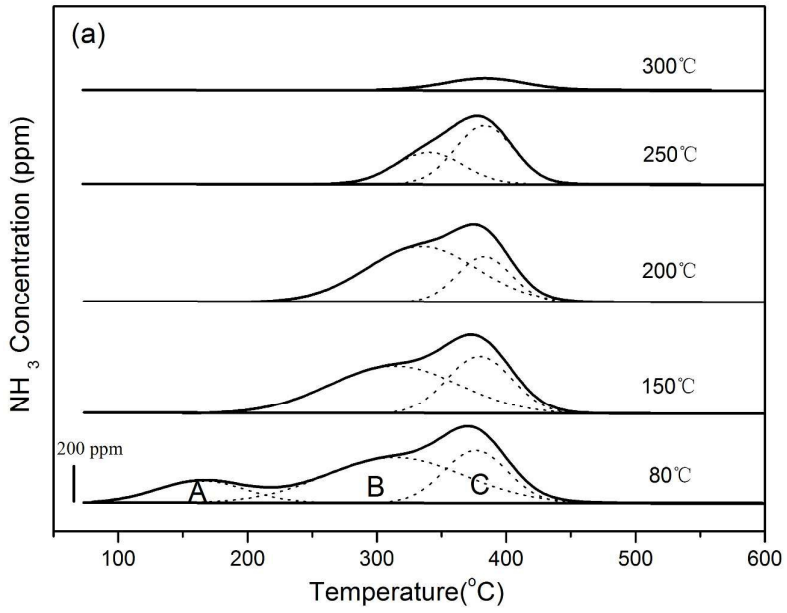

172

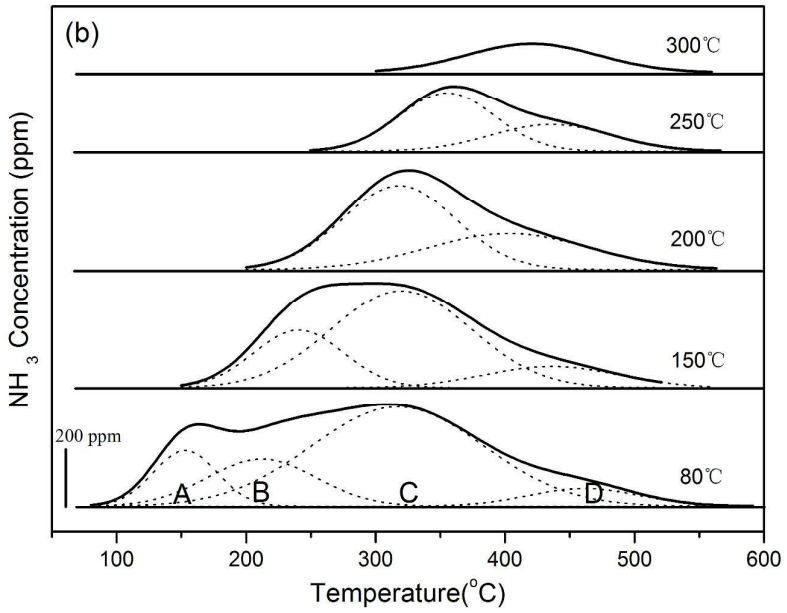

173

Fig. 1 NH_3-TPD profiles of (a) H/SAPO-34 and (b) Cu/SAPO-34 catalyst under different temperatures.

NH_3-TPD is used to determine the amounts and strengths of acid sites over catalysts. Fig. 1 is the deconvolution of NH_3-TPD profiles as a function of temperature under different adsorption temperatures. As shown in the Fig. 1(a), there are three acid sites existing on H/SAPO-34 support, denoted as A, B and C. Low temperature area around 150 ˚C (peak A) is ascribed to NH_3 desorption from weak Brønsted acid sites at surface hydroxyl. Medium and high temperature range (peak B and C) are assigned to the moderate and strong structural Brønsted acid sites. Compared with the TPD results of Cu-SAPO-34 catalyst in Fig. 1(b), more than three acid sites residing in Cu-SAPO-34 catalyst have been discovered. The peak A around 150 ˚C is assigned to the weak Brønsted and Lewis acid sites related to Cu species. The peak B is ascribed to residual structural Brønsted acid sites. Peak C and D above 200 ˚C are considered as strong Brønsted acid sites and the new Lewis acid sites created by the Cu^{2+} species.

Table 1 the fitting results of NH_3-TPD under different temperatures

temperature	sample	weak acid sites (mmol/g)	moderate acid sites (mmol/g)	strong acid sites (mmol/g)
80 ˚C	H/SAPO-34	0.18	0.57	0.30
	Cu/SAPO-34	0.22	0.13	0.87
150 ˚C	H/SAPO-34		0.62	0.28
	Cu/SAPO-34		0.21	0.70
200 ˚C	H/SAPO-34		0.56	0.22

	Cu/SAPO-34	--	0.63
250 ˚C	H/SAPO-34	0.38	0.11
	Cu/SAPO-34	--	0.36
300 ˚C	H/SAPO-34		0.08
	Cu/SAPO-34		0.15
350 ˚C	H/SAPO-34		0.009
	Cu/SAPO-34		0.014

189 The peak quantification results of NH_3-TPD are shown in Table 1. It is seen that NH_3
190 adsorption sites decrease with increase of temperature, while their acidity becomes
191 stronger. Meanwhile, compare with the acid sites of H/SAPO-34 support, the amount
192 of weak and strong acid sites in Cu/SAPO-34 sample increases, while quantity of
193 moderate acid sites decreases. This coincides with assignment of acid sites according
194 to NH_3-TPD profiles.

195 3.1.2 DRIFTS of NH_3 adsorption

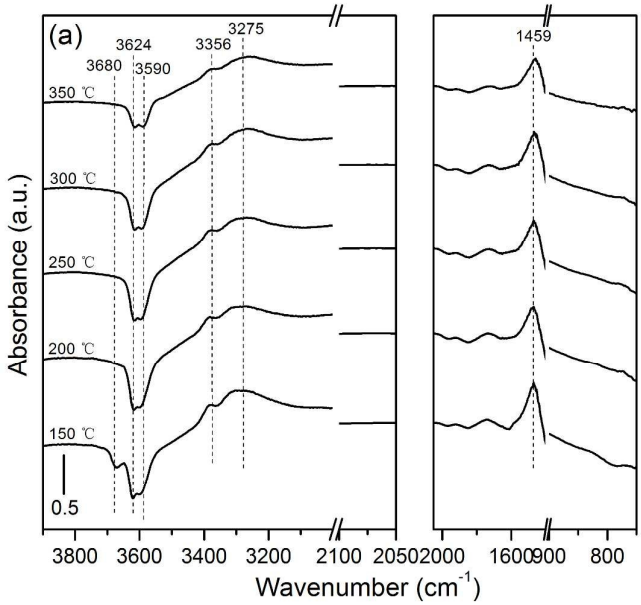

196

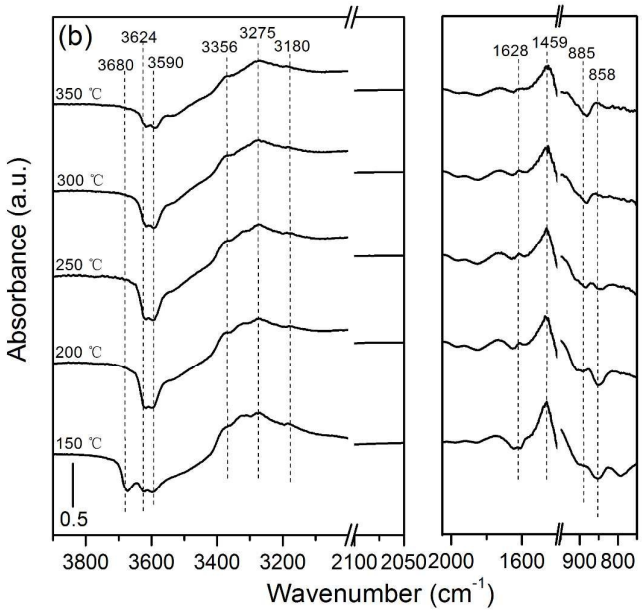

Fig. 2 DRIFTS spectra of NH_3 chemisorbed on (a) H/SAPO-34 and (b) Cu/SAPO-34 catalyst under different temperatures.

The acid sites and their acidity can be further determined using ammonia adsorption DRIFTS.[25] The spectra of adsorbed ammonia on H/SAPO-34 and Cu/SAPO-34 catalyst under different temperatures are shown in Fig. 2. The negative bands at 3680, 3624, and 3590 cm^{-1} are assigned to the OH vibrations of P-OH, Si-OH, and Al-OH-Si, respectively.[22] These bands at 3356, 3275, and 3180 cm^{-1} are due to the N-H stretching vibration of ammonia ions and coordinated ammonia species. In N-H bending vibration region, 1628 and 1459 cm^{-1} are attributed to adsorbed ammonia ions species.[21] And the peak positions and assignments in DRIFTS spectra are listed in the Table 2. Compared with H/SAPO-34 results in Fig. 2(a), new bands at 885 and 858 cm^{-1} appear at Fig. 2(b) over Cu/SAPO-34 sample and they are related to internal asymmetric framework vibrations perturbed by cooper cations to form NH_3-Cu^{2+}.[19, 20, 23, 26] With respect to the similarity in DRIFTS results of H/SAPO-34 support and

Cu/SAPO-34 catalyst, the bands at 3680, 3624, and 3590 cm^{-1} related to Brønsted acid sites are both shown in Figs. 2(a) and 2(b). And the intensities of these bands decrease with the temperature increasing, indicating that the ammonia had desorbed from weak and moderate Brønsted sites. However, strength of 3624, and 3590 cm^{-1} band at each temperature in Fig. 2(b) is lower than that in Fig. 2(a), which means that amount of moderate Brønsted acid sites decreases in Cu/SAPO-34 catalyst. Moreover, the band at 3180 cm^{-1} distinctly decreases above 200 ˚C, which suggests that new weak acid sites formed on Cu/SAPO-34 sample. Additionally, bands at 885 and 858 cm^{-1} assigned to Lewis acid sites have been detected above 300 ˚C only on Cu/SAPO-34. This could result in the increase of strong acid sites. Meanwhile, these consist with NH_3-TPD results that amount of weak and strong sites increases, but quantity of moderate sites decreases. In addition, the IR bands at 3624, 3590 cm^{-1} obviously decrease at 300 ˚C, while the intensity of band at 885 cm^{-1} is still stable with temperature rising above 300 ˚C. Therefore, the ammonia adsorbed on Lewis acid sites is much stronger than that on Brønsted acid sites, uneasily desorbing up to 300 ˚C.

Table 2 peak positions and assignments in the DRIFTS Spectra

Wavenumber (cm^{-1})	Species	Reference
3680, 3624, 3590	P-OH, Si-OH, and Al-OH-Si groups	22
3356, 3275, 3180	N-H stretching vibration	21

1628, 1459	N-H bending vibration	21
885, 858	internal asymmetric framework vibrations perturbed by cooper cations	19,20,23,26

229

230 **3.2 NO_x removal performance**

231 3.2.1 Catalyst characterization

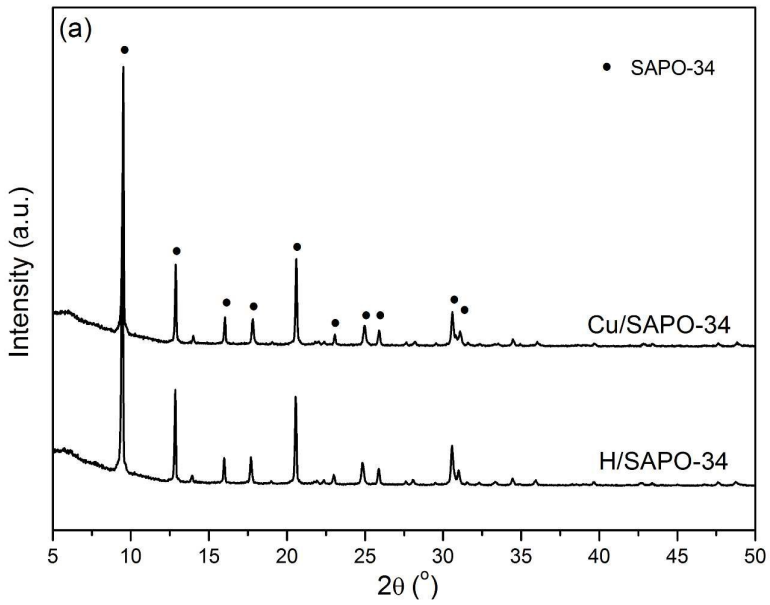

232

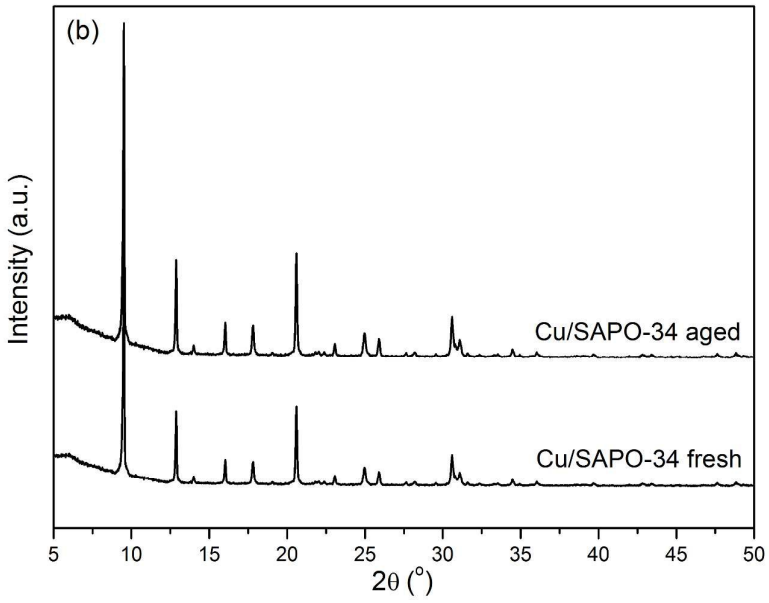

233

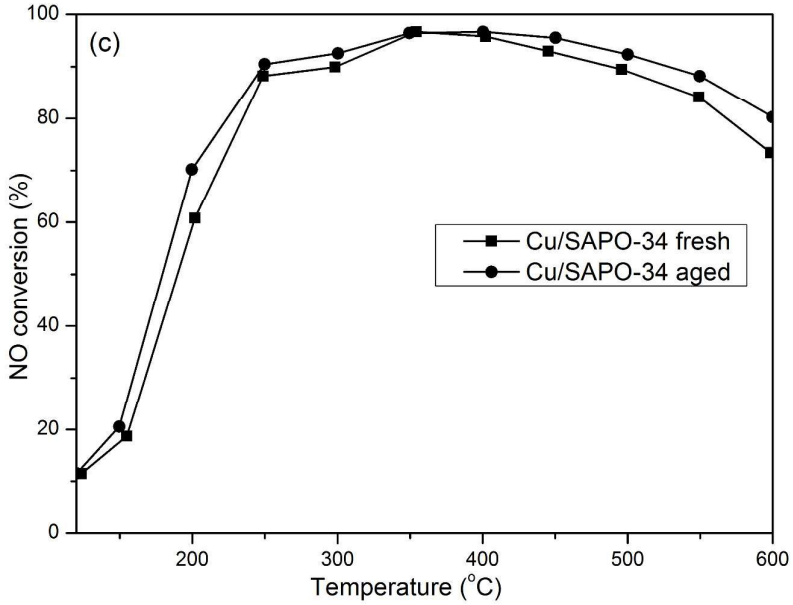

234

235 Fig. 3 (a) XRD patterns of H/SAPO-34 and Cu/SAPO-34, (b) XRD patterns of fresh

236 Cu/SAPO-34 and aged Cu/SAPO-34, (c) de-NO_x activity of fresh Cu/SAPO-34 and aged

237 Cu/SAPO-34

238 Fig. 3 (a) shows the XRD patterns of H/SAPO-34 and Cu/SAPO-34. The diffraction

239 peaks of samples in Fig. 3 (a) are consistent with typical SAPO-34 zeolite, indicating

240 that the prepared SAPO-34 has a CHA structure and the process of Cu loading not

241 destroy the crystalline structure. And the Chemical composition of H/SAPO-34

242 support and Cu/SAPO-34 catalyst are listed in Table 3. Meanwhile, as shown in Fig. 3

243 (b), it shows that the catalyst maintains the intact CHA structure after 750 ˚C, 10%

244 H_2O, 12 h hydrothermal treatment, which suggests its excellent hydrothermal stability.

245 Furthermore, the activity test was performed to probe the de-NO_x performance of the

246 Cu/SAPO-34 catalyst before and after hydrothermal treatment as illustrated in Fig. 3

247 (c). It displays that the aged Cu/SAPO-34 shows higher NO conversion than fresh one,

248 which could results from the increase of isolated Cu^{2+} ions of Cu/SAPO-34 catalyst

249 after hydrothermal treatment. Therefore, whether the structure integrity or SCR
250 activity, the Cu/SAPO-34 catalyst presents excellence performance after hydrothermal
251 treatment.

252 Table 3 Chemical composition of H/SAPO-34 support and Cu/SAPO-34 catalyst

sample	Concentration (w.t. %) (ICP)			
	Al	Si	P	Cu
H/SAPO-34	21.6	8.6	12.3	-
Cu/SAPO-34	21.4	8.6	12.2	1.7

253 3.2.2 De-NO_x efficiency

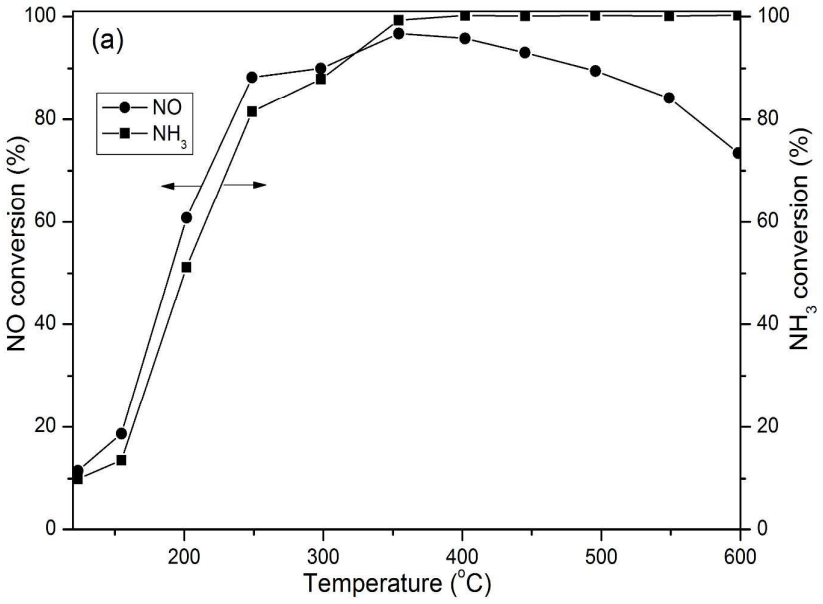

254

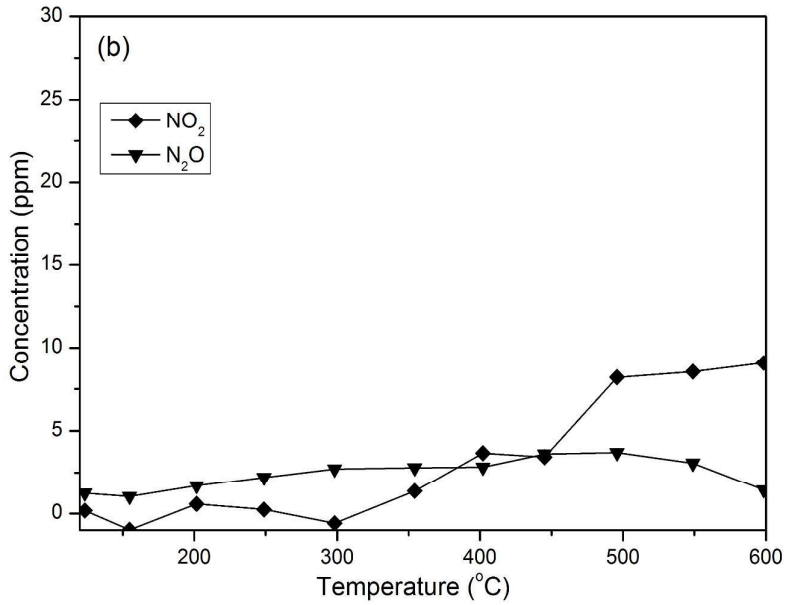

Fig. 4 SCR performance of Cu/SAPO-34 catalyst, Reaction condition: 500 ppm NO, 500 ppm NH_3, 10% O_2, 7% CO_2, 5% H_2O, and N_2 as balance gas. (a) NO conversion and NH_3 conversion; (b) NO_2 and N_2O concentration. Flow rate: 500 ml min^{-1}. GHSV: 300,000 h^{-1}.

In order to examine efficiency of NO_x elimination, the SCR activity was evaluated over Cu/SAPO-34 catalyst from 120 ˚C to 600 ˚C. The NO and NH_3 conversion results are shown in Fig. 4(a). The NO conversion continuously increased and the maximum NO conversion occurred at 350 ˚C. With temperature increasing above 350 ˚C, NO conversion decreased due to the competitive NH_3 oxidation at high temperature. Approximate 100 % NH_3 conversion has been achieved above 350 ˚C. In addition, Fig. 4(b) shows little NO_2 and N_2O were detected during the tests, suggesting high N_2 selectivity. Consequently, the homemade Cu/SAPO-34 catalyst with representative SCR performance could be used to study the behavior of various reactants, which is guarantee of current passive-SCR research.

3.2.3 Lean NO_x reaction performance with adsorbed ammonia

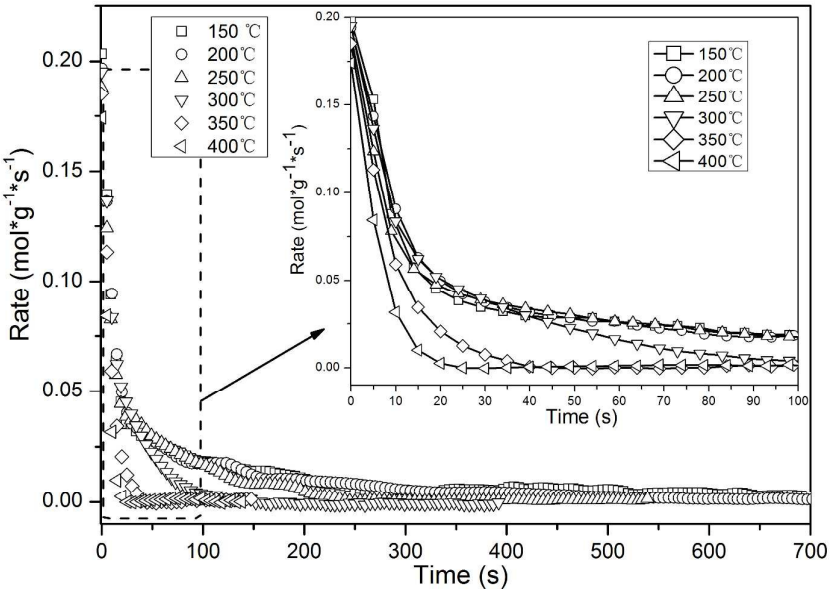

Fig. 5 SCR rates as function of time at different temperatures over Cu-SAPO-34 catalyst.

At lean period of passive-SCR process, NH_3 saturated catalyst is actually titrated by generated NO_x. In order to evaluate the activity of adsorbed NH_3 species, they were titrated by $NO+O_2$ under a series of temperatures in Fig. 5. At the first dozens of seconds, NO conversion rates rapidly decrease under all temperatures. And with the proceeding of the reaction, NO reaction rates show distinctly different performance with the former. Moreover, the lower the reaction temperature is, the longer the equilibrium needs. When temperature is above 300 ˚C, it is shown that adsorbed NH_3 could be thoroughly consumed within 100 seconds. However, reaction equilibrium needs a long time to reach below 300 ˚C. Consequently, different activity of adsorbed NH_3 along with time could imply that there are diverse mechanisms under corresponding temperature.

283 3.2.4 DRIFTS spectra of Lean NO_x reaction with adsorbed ammonia

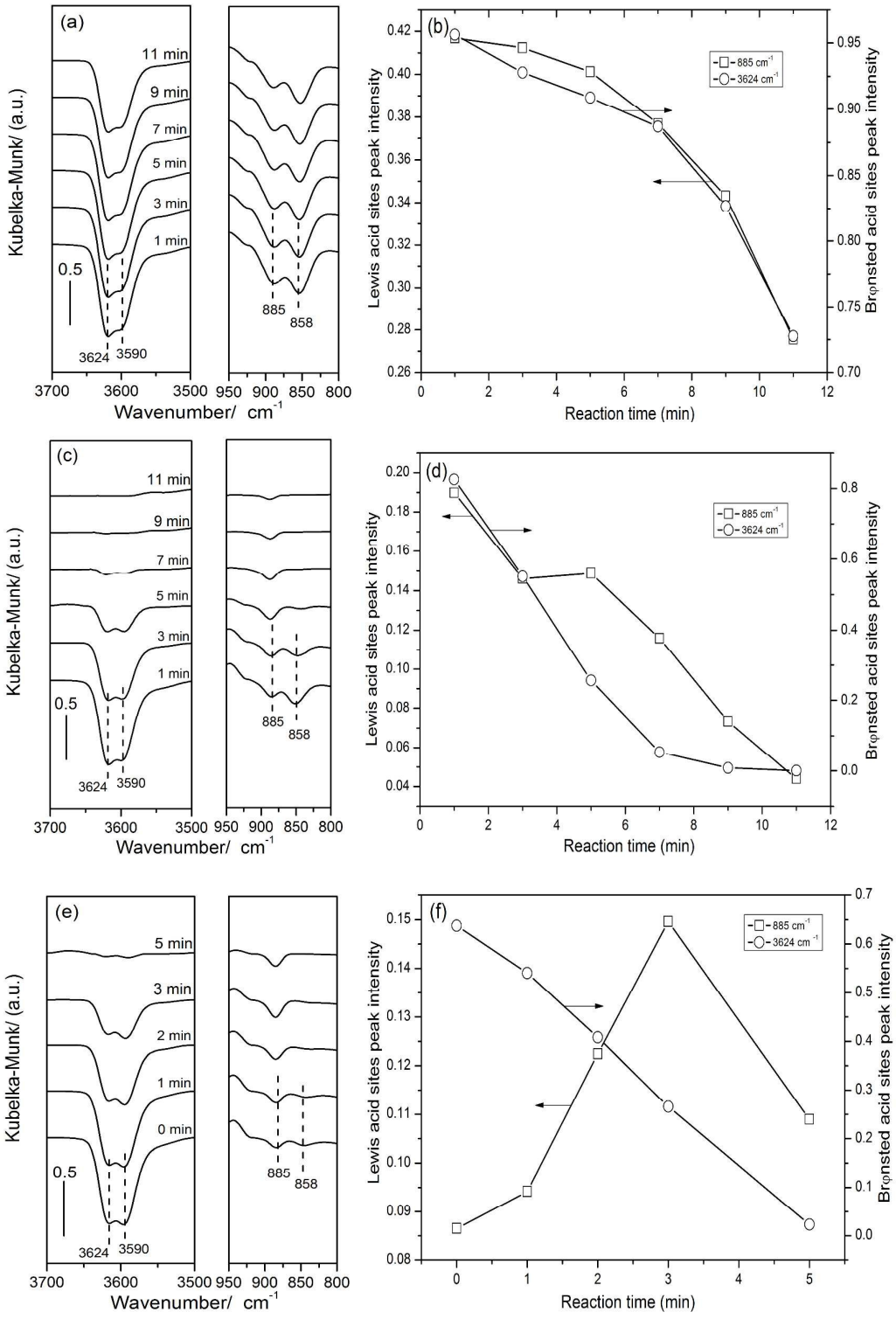

284

285

286

287

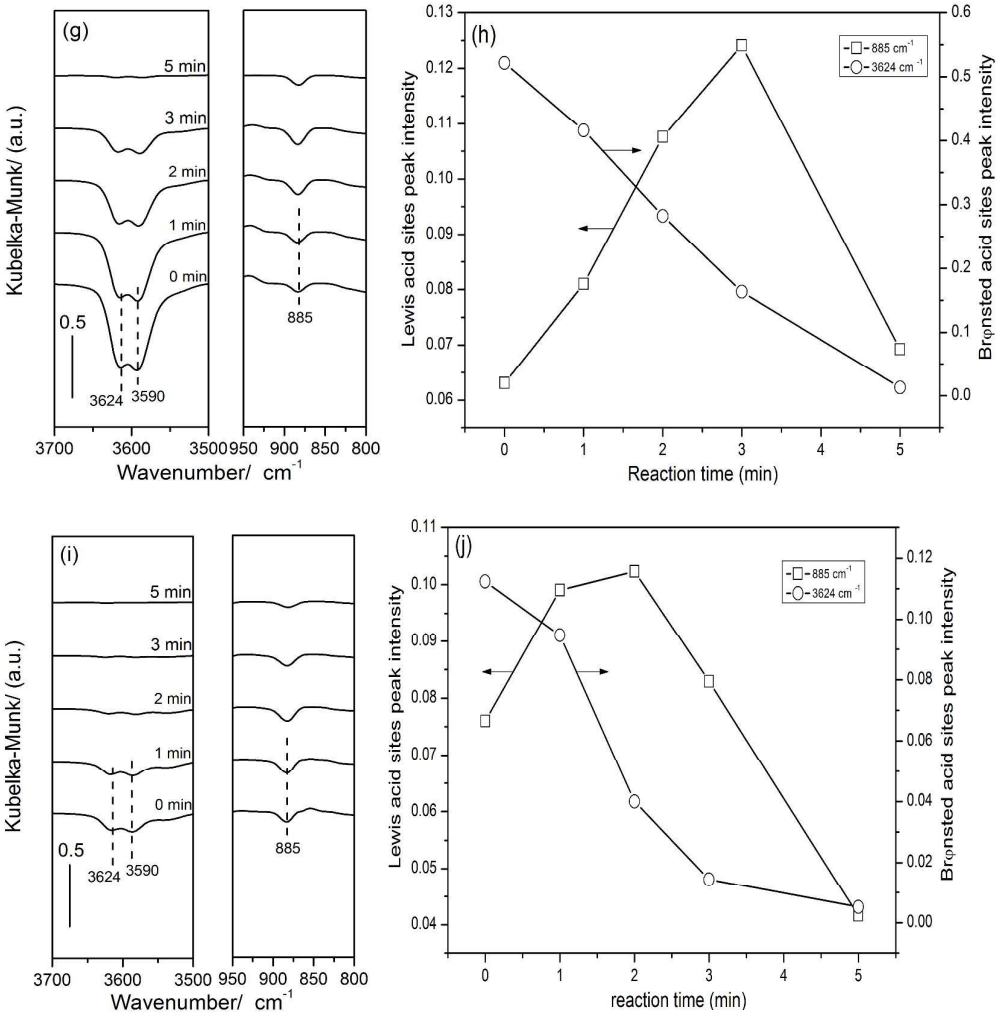

Fig. 6 $NO+O_2$ titration experiment was performed at 150 ˚C (a), 200 ˚C (c), 250 ˚C (e), 300 ˚C (g), 350 ˚C (i). Left parts: DRIFTS spectra of adsorbed NH_3 titration by $NO+O_2$ on Cu-SAPO-34 at different time (0 min, 1 min, 2 min, 3 min, 5 min and 7 min, 9 min, 11 min). Right parts: the change of peak intensity of representative Lewis and Brønsted acid sites during the $NO+O_2$ titration (b), (d), (f), (h), and (j).

The DRIFTS spectra of adsorbed NH_3 titration by $NO+O_2$ at a series of temperatures (150, 200, 250, 300, 350 ˚C) are shown in Fig. 6. Particularly, the blank experiment was carried out to rule out the effect of residual NH_3 in system and verify their

298 reliability. The results were shown in Figs. S2 and S3. As reported previously,[22] the
299 doublet bands at 3624 cm^{-1} and 3590 cm^{-1} were assigned to the stretching model of
300 bridged Brønsted OH groups Al-(OH)-Si, which could represent the Brønsted acid
301 sites. Meanwhile, the bands at 885 and 858 cm^{-1} were related to Lewis acid sites of
302 Cu^{2+}ions. Accordingly, the peak intensity of 3624 cm^{-1} and 885 cm^{-1} in DRIFTS
303 spectra are chosen to study the behaviors of adsorbed ammonia species on the
304 Cu-SAPO-34 catalyst. Peak intensity, representing the ammonia contents, are plotted
305 in Fig. 6 (b), (d), (f), (h), and (j), respectively. As it is shown in Figs. 6(b) and 6(d),
306 the peak intensity of Brønsted acid sites and Lewis acid sites simultaneously
307 decreases with proceeding of titration reaction at relative low temperature (150 ˚C and
308 200 ˚C). However, when reaction temperature increases, Brønsted acid sites intensity
309 still decreases along with time. But Lewis acid sites increases at initial two minutes
310 and follows an abruptly decreases. Moreover, since Cu^{2+} cations (Lewis acid sites) are
311 SCR reaction active sites, adsorbed NH_3 could be directly consumed on Cu^{2+} cations
312 of Cu/SAPO-34 catalyst. This results in the decrease of peak intensity of Lewis acid
313 sites. Subsequently, NH_3 adsorbed on Brønsted acid sites have to migrate from
314 Brønsted acid sites to Lewis acid sites for participation in SCR reaction. Consequently,
315 the increase of adsorbed ammonia on Lewis sites is due to the NH_3 migration from
316 Brønsted sites. In view of above results, it suggests that NH_3 migration between two
317 acid sites, potentially enabling NH_3 to be transferred to Lewis acid sites and reacted.
318 The different variation trend of adsorbed ammonia contents on Lewis sites at different

temperature range is related to the speed of NH_3 consumption and NH_3 migration, which will be discussed later. In a word, rate difference of NH_3 migration and reaction bring about the different performance of adsorbed NH_3 in titration reaction.

3.3 The kinetic results

3.3.1 Reaction kinetics results

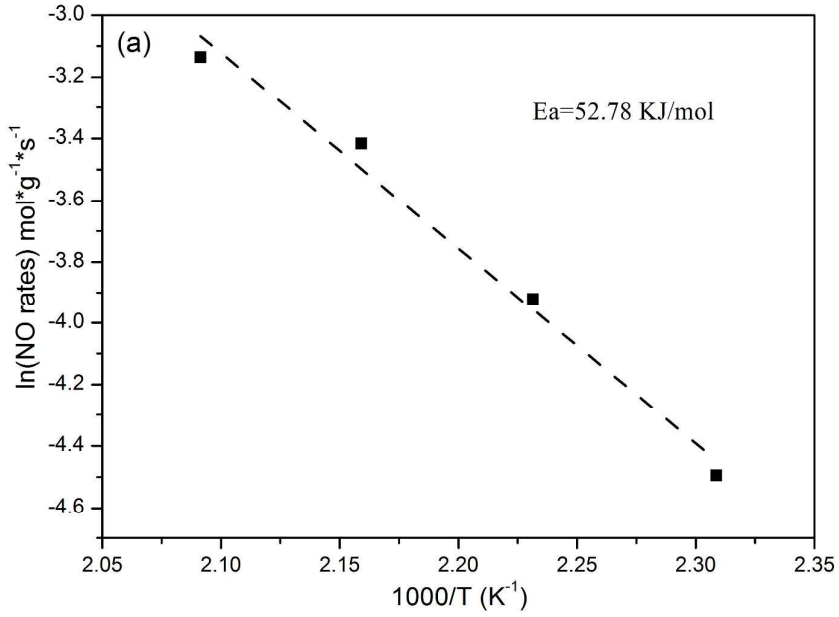

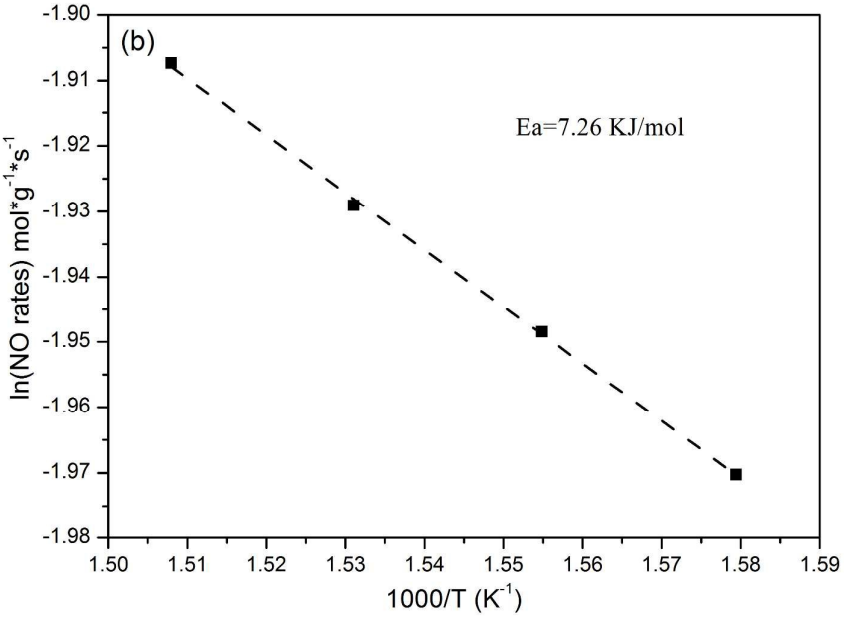

Fig. 7 Arrhenius plots of the SCR reaction rates per gram Cu/SAPO-34 at 160-205 ˚C (a), and 360-390 ˚C (b). Condition: 500 ppm NO, 500 ppm NH_3, 5% O_2, and N_2 as balance gas. Flow rate: 1.5 l min^{-1}. GHSV: 3,600,000 h^{-1}.

In order to contrast difficulty of NH_3 migration and reaction over Cu/SAPO-34 catalyst, it is possible to compare the reaction activity energy with adsorption energy. Consequently, SCR activity energy and NH_3 adsorption energy on Cu/SAPO-34 sample could be calculated in the following section. And NH_3-SCR reaction rate equation could be expressed as following equation:

$$r = k\ C_{NH_3}^{\alpha} C_{NO}^{\beta} C_{O_2}^{\theta} \quad (5)$$

On the basis of our previous results, SCR reaction order for NH_3, NO, and O_2 is approximately 0, 1, and 0.5.[27] As a result, $\alpha=0$，$\beta=1$，$\theta=0.5$ are taken into the rate equation and simplified as follow:

$$\ln r = \ln k + \ln C_{NO} + 0.5 \ln C_{o_2} \quad (6)$$

Because the reactant concentrations in present research are C_{NO}=500 ppm and C_{O2}=5%, then the Arrhenius equation can be introduced into Eq (6). And the simplified Eq (6) was obtained through above calculation. Consequently, Arrhenius plots of the SCR reaction rates are attained from simplified Eq (6), as shown in Fig. 7. Thereupon, SCR reaction Ea can be calculated through Arrhenius plots, from which Ea at low temperature and high temperature are obtained as 52.78 KJ/mol and 7.26 KJ/mol for Cu/SAPO-34 catalyst.[28]

346 3.3.2 NH_3 adsorption kinetics results

347 The adsorption energy of NH_3 can be obtained from the Langmuir isotherm model
348 incorporating temperature dependency. The concentration of NH_3 (Q_S) presenting in
349 the fully filled micro-pores of a material can be calculated from:

350 $$Q_s = M_p / V_* \quad (7)$$

351 Where M_p (cm^3/g) is the micropore volume of the material, and V_* (cm^3/mol) is the
352 mole volume of NH_3 at the adsorption temperature. The molar volume can be
353 calculated from Virial equation of state, as described previously.[29] The Langmuir
354 model equation, considering temperature dependency of K_a, is expressed as:

355 $$Q = (Q_S K_a P) / (1 + K_a P) \quad (8)$$

356 where $K_a = K_{a0} \exp(q/RT)$

357 Q (mmol/g) is the amount of adsorbate. Ka (1/pa) is an equilibrium parameter. Ka_0
358 (1/pa) is an equilibrium constant. q (KJ/mol) is the adsorption energy. R is the ideal
359 gas constant. P (pa) is the gas pressure. T (K) is adsorption temperature.

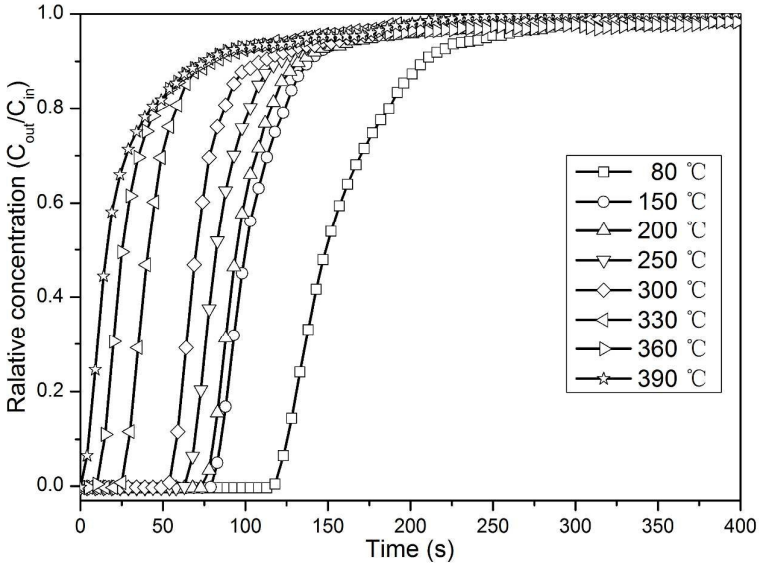

Fig. 8 the NH_3 breakthrough curves at different temperatures on Cu-SAPO-34 catalyst

Table 4 Adsorption amount of NH_3 on Cu/SAPO-34 catalyst at saturation

catalyst	adsorbate	Adsorption temperatures (˚C)	Amount of adsorbed NH_3 (mmol/g)
Cu/SAPO-34	NH_3	80	1.316
	NH_3	150	0.944
	NH_3	200	0.587
	NH_3	250	0.288
	NH_3	300	0.101
	NH_3	330	0.048
	NH_3	360	0.013
	NH_3	390	0.009

Fig. 8 displays the NH_3 breakthrough curves for Cu-SAPO-34 catalyst at different temperatures (80, 150, 200, 250, 300, 330, 360 and 390 ˚C). The relative NH_3 concentration, the ratio of outlet concentration (C_{out}) to inlet concentration (C_{in}), as a function of time was plotted in Fig. 8. A relative concentration value of 1 implies NH_3

adsorption saturation on the catalyst. The breakthrough time are shortened with increase of adsorption temperature, indicating that the amount of NH_3 adsorption site decreases.[30] The amount of adsorbed NH_3 is determined by the temperature program desorption from test temperature to 600 ˚C and the results are listed in Table 4. Fig. 9 depicts the temperature dependence of the calculated adsorption equilibrium parameter (Ka), from which adsorption energy of 12.22 and 87.54 kJ/mol are obtained.

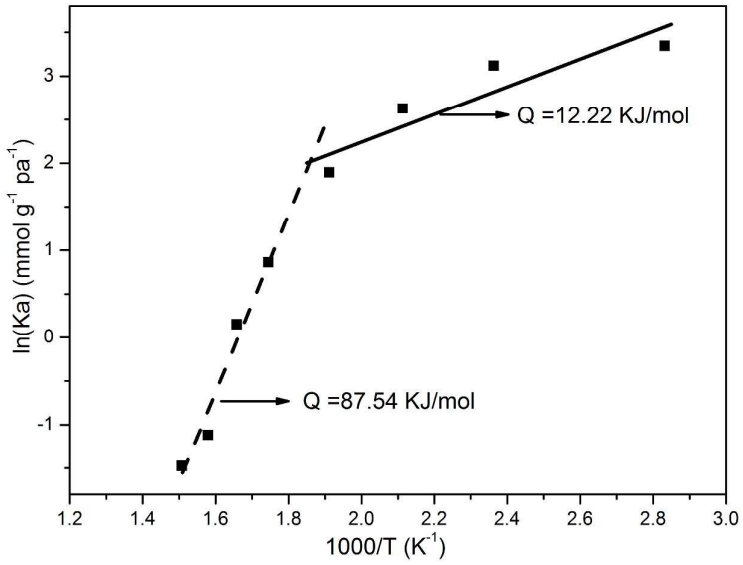

Fig. 9 The adsorption equilibrium parameter of NH_3 under Langmuir isotherm model on Cu/SAPO-34 sample

4. Discussion

4.1 NH_3 adsorption performance and Assignment of various adsorption sites on Cu/SAPO-34 catalyst

In order to understand the NH_3 behavior during passive-SCR process, the acid type and Cu influence on acid sites of catalyst should be clearly separated firstly.

382 Comparing the NH_3-TPD results of H/SAPO-34 support and Cu/SAPO-34 catalyst in
383 Fig. 1, it is shown that weak and strong acid sites amount in later one increases, but its
384 moderate acid sites decrease. This is also verified by peak quantification results of
385 NH_3-TPD under each temperature. For Cu/SAPO-34 sample, the increase of weak and
386 strong acid sites amount in Table 1 results from Cu species incorporation into
387 H/SAPO-34 support. As illustrated in Fig. 2(b), band at 3180 cm^{-1} is due to the N-H
388 stretching vibration of coordinated ammonia species (NH_3-Cu^{+}) , which desorbs at
389 low temperature and is attributed to weak Lewis acid sites. Meanwhile, the bands at
390 885 and 858 cm^{-1} are related to NH_3-Cu^{2+}, which is assigned to strong Lewis acid
391 sites. Conversely, amount of moderate acid sites decreases on the Cu/SAPO-34
392 sample compared with H/SAPO-34 support. This is induced by replacement of
393 Brønsted hydroxyl in Si-OH-Al groups by Cu species. The bands at 3624 and 3590
394 cm^{-1} are attributed to OH vibrations of Al-OH-Si structure. And the strength of these
395 two negative peak decreases in Cu/SAPO-34 sample. This verifies the speculation
396 about decrease of moderate acid sites. Furthermore, comparing NH_3-TPD profiles of
397 different temperatures in Fig. 1(b), the quantity and species of adsorbed NH_3 on
398 Cu/SAPO-34 sample gradually decrease with increasing of temperature. Specifically,
399 amount of adsorbed NH_3 on Brønsted acid sites quickly decrease, however the NH_3
400 adsorbed on Lewis acid sites seldom desorb at high temperature. NH_3 adsorption
401 DRIFTS in Fig. 2(b) illustrates that bands at 3624, 3590 cm^{-1} related to Brønsted acid
402 sites significantly decrease, nevertheless band at 885 cm^{-1} attributed to Lewis acid

403 sites scarcely changes above 300 ˚C. Consequently, strong Lewis acid sites related to
404 Cu^{2+} species could play a more important role in NH_3 adsorption process at high
405 temperature. Furthermore, in passive-SCR process, generated NH_3 in rich period need
406 be adsorbed as much as possible, especially at high temperature. Accordingly, for
407 fulfilling the different NH_3 adsorption requirements of passive-SCR in future, it is
408 possible to attain specific catalyst formula by modulating the Cu content, Si content
409 and templates. After rich period of passive-SCR process, in order to examine the
410 performance of Cu/SAPO-34 catalyst in lean period, it is necessary to discuss reaction
411 behavior of adsorbed NH_3 below.

412 **4.2 Activity of various adsorbed NH_3 species over Cu/SAPO-34**

413 Combined the NH_3-TPD results, there is just Brønsted site on H/SAPO-34, while both
414 Brønsted site and Lewis site exist on Cu/SAPO-34. It is known that H/SAPO-34
415 almost performs no SCR activity, and Lewis site is SCR active site. Therefore, Lewis
416 site is active in SCR reaction and NH_3 adsorbed on Lewis sites is denoted as active
417 NH_3 species, while those adsorbed on Brønsted site are labeled as inactive NH_3
418 species. And inactive NH_3 should transform into active NH_3 by NH_3 migration to
419 Lewis site, sequently participates in SCR reaction. Furthermore, active and inactive
420 NH_3 species present different reaction behavior at low and high temperature in
421 titration reaction. Consequently, it is important to discuss the problem of NH_3
422 migration and SCR reaction rate of various adsorbed NH_3. As shown in Figs. 6(b) and
423 (d), amount of active and inactive NH_3 both declines at low temperature, which

424 suggests that migration rate of inactive NH_3 is slower than reaction rate of active NH_3.
425 Moreover, this is the explanation that reaction equilibrium reached in a long time at
426 low temperature in Fig. 5. However, quantity of active NH_3 shows a short increase
427 before decrease with inactive NH_3 at high temperature in Figs. 6(f), (h) and (j). And it
428 illustrates that migration rate of inactive NH_3 is faster than reaction rate of active NH_3.
429 Therefore, adsorbed NH_3 is rapidly consumed at high temperature as shown in Fig. 5.
430 Furthermore, it is necessary to combine the NH_3 adsorption strength on Cu/SAPO-34
431 and systematically discuss its application potential in lean and rich operation of
432 passive-SCR technology. Meanwhile, possible mechanism of passive-SCR could be
433 proposed.

434 **4.3 Reaction mechanism of passive-SCR process**

435 Considering the efficiency of passive-SCR process, the discussion about controlling
436 factors and rate-determining step during different periods is essential for Cu/SAPO-34
437 application and modification in future. It is known that the front TWC catalyst and
438 back SCR catalyst satisfy the exhaust elimination in different periods. In this study,
439 we focus on the role of back SCR catalyst and the potential of Cu/SAPO-34 sample.
440 During rich period, NH_3 is generated over front TWC catalyst and stored on back
441 SCR catalyst. And the acid content and acidity of Cu/SAPO-34 sample are the main
442 factor to adsorb NH_3, which ensure to prevent the secondary pollution for NH_3 slip.
443 During lean period, the generated NO from the front TWC could be consumed by
444 NH_3 saturated Cu/SAPO-34 sample. Consequently, the activity of adsorbed NH_3

445 species and the NH_3 consumption rate-determining step are key point to understand.
446 For Cu/SAPO-34 catalyst, the NH_3 adsorption only happens during rich period.
447 NH_3-TPD results in Fig. 1 and Table 1 show its excellent NH_3 adsorption capacity.
448 Since that the NH_3 adsorption sites decrease with increasing of temperature, our
449 previous study found that Cu/SAPO-34 acidity could be adjusted to modify the Si
450 contents, Cu contents and templates for the detailed engine requirement. In addition,
451 the NH_3 consumption mechanism over Cu/SAPO-34 sample during lean period is
452 shown in Scheme 1. Figs. 5 and 6 present the inactive NH_3 species on Brønsted sites
453 have to become active NH_3 species on Lewis sites to participate in NO consumption
454 reaction, since the Cu^{2+} species are the only active site for SCR over Cu/SAPO-34
455 sample. Due to the variation of NH_3 adsorption energy and apparent activation energy
456 at different temperature range, the rate-determining step changes at lean period. At
457 low temperature, Fig. 6 presents the NH_3 migration is slower than NH_3 consumption
458 on active sites and NH_3 could be easily adsorbed on acid sites. Compared with the NO
459 consumption rate, the passive-SCR reaction is controlled by the NH_3 migration as
460 shown in Scheme 1a. In addition, the NH_3 adsorption energy in Fig. 9 could be
461 approximately ascribed to NH_3 adsorption on Brønsted acid sites (12.22 kJ/mol) and
462 Lewis acid sites (87.54 kJ/mol), since the Lewis acid sites show the strongest acidity
463 in Fig. 1 at high temperature and NH_3 mainly adsorbs on Brønsted sites for its
464 overwhelming contents at low temperature. Therefore, their differences (75.32 kJ/mol)
465 is the apparent energy of migration from Brønsted acid sites to Lewis acid sites,

466 which is higher than NO consumption apparent Ea in Fig. 7(a). This also proves that
467 NH_3 migration is the rate-determining step at low temperature. The increase of Lewis
468 acid sites could improve the passive-SCR efficiency at low temperature. At high
469 temperature range, Fig. 6 reveals the NH_3 migration performs higher speed than NO
470 consumption rate on Cu^{2+} sites and the apparent Ea value in Fig. 7(b) also shows the
471 fast rate of NO consumption at high temperature. As is shown in Scheme 1(b), the
472 efficient adsorbed NH_3 activity could ensure the NO consumption over Cu/SAPO-34
473 sample, while the decreasing NH_3 adsorption sites are the main factor to the
474 passive-SCR process at high temperature. Consequently, NH_3 adsorption may be the
475 rate-determining step of passive-SCR rich period under high temperature.

476 Furthermore, compared with standard NH_3-SCR mechanism,[22, 31] the distinction of
477 passive-SCR process is its different rate-determining step. In view of the NH_3-SCR
478 process, the orders of reactant NH_3 and NO over Cu/SAPO-34 were 0 and 0.75,
479 respectively. And it suggests that NH_3 species adsorption is easy and strong, but it is
480 difficult for NO species.[27] Therefore, it is proposed that the NH_3-SCR reaction
481 mechanism tends to be E-R mechanism. And our previous works proved that isolated
482 Cu^{2+} are the active sites for NH_3-SCR reaction under 200 °C.[32] Furthermore, it is
483 reported that ammonia nitrites are the intermediates and decompose to nitrogen and
484 water.[22, 23] And the rate-determining step of NH_3-SCR mechanism is still controversial
485 up to now. Actually, both NH_3-SCR and passive-SCR process are coincident in term
486 of the essence of NH_3-SCR reaction. And the passive-SCR process is deemed as the

stepwise NH_3-SCR, in which the effect of NH_3 adsorption is ruled out. Because after catalyst saturated by NH_3 in rich period, the adsorbed NH_3 was reacted through static consumption process during lean period without NH_3 supplement. Moreover, it could present the same adsorption species and intermediates as standard NH_3-SCR, while it shows different rate-determining steps. The NH_3 migration plays a vital role in passive-SCR process, which could be the rate-determining step of low temperature in leap period. In short, the significance of NH_3 migration in NH_3-SCR reaction could be distinctly reflected in the passive-SCR research.

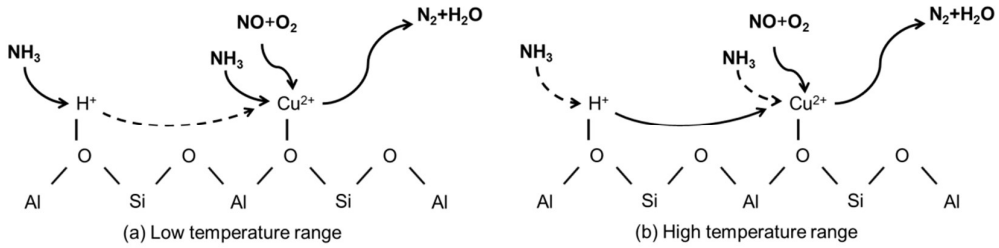

Scheme 1 mechanism of passive-SCR process over Cu/SAPO-34 catalyst (a) at low temperature range, (b) at high temperature range

5. Conclusion

The acid sites assignment and activity of various adsorbed NH_3 species over Cu/SAPO-34 catalyst have been studied systematically. NH_3-TPD and DRIFTS results illustrate SAPO-34 support contains different Brønsted acid sites and Cu incorporation creates Lewis acid sites in Cu/SAPO-34 sample. The amount of weak and strong acid sites over Cu/SAPO-34 sample increases, which results from Cu incorporation forming Lewis sites. However, due to replacement of Brønsted

505 hydroxyl in Si-OH-Al groups by Cu^{2+} species, quantity of moderate acid sites
506 decreases. Furthermore, possible reaction mechanism and rate-determining step of
507 passive-SCR process are proposed. Firstly, active NH_3 adsorbed on Lewis sites
508 presents high activity, but inactive NH_3 species have to migrate and transform into
509 active NH_3 for NO consumption. For the rich period of passive-SCR, only NH_3
510 adsorption happens and the increase of acid sites could satisfy the different technical
511 requirement. For the lean period, inactive NH_3 migration rate from Brønsted acid sites
512 to Lewis acid sites is slower than NO consumption rate by active NH_3, which confines
513 the SCR reaction rate at low temperature. Therefore, NH_3 migration could be the
514 rate-determining step of passive-SCR lean period during low temperature range.
515 Nevertheless, at high temperature, NH_3 migration presents high speed than NO
516 consumption rate and the adsorbed NH_3 species reveal enough activity for NO
517 consumption. While the decreasing NH_3 adsorption sites are the main effect on the
518 passive-SCR process at high temperature. Accordingly, the rate-determining step of
519 passive-SCR rich period during high temperature range is the adsorption of NH_3.

520 **Acknowledgement**

521 The authors are grateful to the financial support from the GM Global Research &
522 Development (RD-07-312–NV487). This work was supported by the program of the
523 National High Technology Research and Development Program of China (863
524 Program, 2011AA03A405).

Notes and References

1. W. Li, K. Perry, K. Narayanaswamy, C. Kim and P. Najt, SAE International, 2010-01-0366.

2. O. Guralp, G. Qi, W. Li, P. Najt, SAE International, 2011-01-0307.

3. C. Kim, K. Perry, M. Viola, W. Li, K. Narayanaswamy, SAE International, 2011-01-0306.

4. J. Wang, Y. Ji, G. Jacobs, S. Jones, D. Kim, M. Crocker, Appl. Catal. B, 2014, 148-149, 51-61.

5. B. Shakya, M. Harold, V. Balakotaiah, Chem. Eng. J., 2014, 237, 109-122.

6. Y. Liu, Y. Zheng, M. Harold, D. Luss, Top Catal., 2013, 56, 104-108.

7. F. Rohr, D. Peter, E. Lox, E. Kögel, A. Sassi, L. Juste, C. Rigaudeau, G. Belot, P. Gélin, M. Primet, Appl. Catal. B, 2005, 56, 201-212.

8. S. Matsumoto, Y. Ikeda, H. Suzuki, M. Ogai, N. Miyoshi, Appl. Catal. B, 2000, 25, 115-124.

9. I. Bull, W. Xue, P. Burk, S. Boorse, W. Jaglowski, G. Koermer, A. Moini, J. Patchett, J. Dettling, M. Caudle, US patent, 2009, US 7,601,662 B2.

10. T. Ishihara, M. kagawa, F. Hadama, Y. Takita, J. Catal., 1997, 169, 93-102.

11. D. Fickel, E. D'Addio, J. Lauterbach, R. Lobo, Appl. Catal. B, 2011, 102, 441-448.

12. Q. Ye, L. Wang, R. Yang, Appl. Catal. A, 2012, 427-428, 24-34.

13. R. Martínez-Franco, M. Moliner, C. Franch, A. Kustov, A. Corma, Appl. Catal. B, 2012, 127, 273-280.

14. S. Gómez, A. Campero, A. Hernández, G. Fuentes, Appl. Catal. A, 2000, 197, 157-164.

15. J. Kryca, M. Iwaniszyn, M. Piatek, P. Jodlowski, J. Thomas, A. Kolodziej, J. Lojewska, Catal. Today, 2013, 216, 135-141.

16. J. Wang, Z. Peng, H. Qiao, L. Han, W. Bao, L. Chang, G. Feng, W. Liu, RSC Adv., 2014, 4, 42403.

17. J. Wang, T. Yu, X. Wang, G. Qi, J. Xue, M. Shen, W. Li, Appl. Catal. B, 2012, 127, 137-147.

18. X. Hou, S. Schmieg, W. Li, W. Epling, Catal. Today, 2012, 197, 9-17.

19. P. Fanning, M. Vannice, J. Catal., 2002, 207, 166-182.

20. L. Wang, G. Qi, D. Weng, J. Catal., 2012, 289, 21-29.

21. L. Ma, Y. Cheng, G. Cavataio, R. McCabe, L. Fu, J. Li, Appl. Catal. B, 2014, 156-157, 428-437.

22. D. Wang, L. Zhang, K. Kamasamudram, W. Epling, ACS Catal., 2013, 3, 871-881.

23. L. Shi, T. Yu, X. Wang, J. Wang, M. Shen, Acta Phys-Chim Sin, 2013, 29(7), 1550-1557.

24. T. Yu, J. Wang, M. Shen, W. Li, Catal. Sci. Technol., 2013, 3, 3234-3241.

565 25. L. Ma, J. Li, R. Ke, L. Fu, J. Phys. Chem. C, 2011, 115, 7603-7612.

566 26. G. Lei, B. Adelman, J. Sárkány, W. Sachtler, Appl. Catal. B, 1995, 5, 245-256.

567 27. T. Yu, T. Hao, D. Fan, J. Wang, M. Shen, W. Li, J. Phys. Chem. C, 2014, 118 (13),

568 6565–6575.

569 28. I. Centeno, S. Castillo, R. Camposeco, G. Fuentes, Catal. Commun, 2013, 31,

570 11-15.

571 29. D. Kim, J. Wang, M. Crocker, Catal. Today, 2014, 231, 83-89.

572 30. G. Wang, B. Dou, J. Wang, W. Wang, Z. Hao, RSC Advances, 2013, 3, 20523.

573 31. C. Paolucci, A. A. Verma, S. A. Bates, V. F. Kispersky, J. T. Miller, R. Gounder, W.

574 N. Delgass, F. H. Ribeiro, W. F. Schneider, Angew. Chem. Int. Ed. 2014, 53, 1-7

575 32. J. Xue, X. Wang, G. Qi, J. Wang, M. Shen, W. Li, Journal of Catalysis 297 (2013)

576 56–64.